INT. J. REMOTE SENSING, 1991, VOL. 12, NO. 10, 2045–2063

Testing the utility of simple multi-date Thematic Mapper calibration algorithms for monitoring turbid inland waters

RICHARD G. LATHROP†, THOMAS M. LILLESAND

Environmental Remote Sensing Center, University of Wisconsin-Madison, 1225 W. Dayton St., Madison, Wisconsin 53707, U.S.A.

and BRIAN S. YANDELL

Statistics Department, University of Wisconsin-Madison 1210 W. Dayton St., Madison, Wisconsin 53706, U.S.A.

(Received 20 July 1989; in final form 3 January 1990)

Abstract. This study reports on an investigation of multi-date water-quality calibration algorithms under turbid inland water conditions using Landsat Thematic Mapper (TM) multispectral digital data. TM data and water-quality observations were obtained near-simultaneously in Green Bay, an embayment of Lake Michigan, and related using linear regression techniques. The high concentrations of terrestrially-derived suspended solids appear to be controlling the water volume reflectance. A simple exponential model using the band 3/band 1 (0·660 μm/0·485 μm) ratio was found to be a useful index for estimating total suspended solids and water transparency (i.e. Secchi disk depth) with an accuracy of ± 25 per cent over the calibration data range.

1. Introduction

Monitoring the water quality of inland lake systems presents both a challenge to and opportunity for the application of satellite remote sensing. Natural lake water is optically complex due to covarying concentrations of three main constituents: inorganic suspended solids (SS); phytoplankton pigments (e.g. chlorophyll-a); and dissolved organic matter (DOM). Mechanistic understanding of the relationship between water constituent concentrations, water volume reflectance and satellite sensor-observed radiance through radiative transfer modelling provides the most rigorous basis for calibrating water-quality estimation algorithms. This mechanistic approach requires a complete spectral characterization of the absorption and backscattering properties of water and its constituents, as well as modelling radiative transfer across the air/water interface and the intervening atmosphere (Bukata *et al.* 1985, Gordon and Morel 1983). Owing to the optical complexity of turbid waters, no individual constituent estimation algorithm derived from first principles has yet been developed, but it is an active area of both marine and inland water research (Carder *et al.* 1989, Bukata *et al.* 1988).

Based on a fundamental understanding of the optical characteristics of a water body and its main constituents, an empirical calibration approach uses regression

†Present Address: Department of Environmental Resources, College Farm Road, Cook College-Rutgers University, New Brunswick, New Jersey 08903, U.S.A.

analysis to relate statistically the volume reflectance to the parameter of interest. Though more complicated in many respects, turbid inland water bodies with covarying SS, chlorophyll-a, and DOM levels actually help to simplify matters because SS in moderate to high concentrations strongly backscatter light and tend to dominate the water volume reflectance (Bukata *et al.* 1988, Holyer 1978). Though the estimation of phytoplankton pigment concentrations is problematic in turbid lake waters, the estimation of SS concentration and more general measures of water transparancy (e.g. Secchi disk depth) are possible using the limited spectral resolution afforded by such relatively broad-band sensors as the Landsat Multispectral Scanner (MSS) and Landsat Thematic Mapper (TM) (Curran and Novo 1988). Though limited in their universal application (i.e. extrapolation to conditions other than those under which they were calibrated), empirically derived algorithms can provide a reasonable degree of predictive accuracy (Whitlock *et al.* 1982).

In an earlier study, Lathrop and Lillesand (1986) demonstrated the potential utility of TM digital data in mapping turbid inland water quality. These initial results prompted further research emphasizing the identification of simple calibration algorithms for a multi-date TM reflectance/water-quality data set, which is the subject of this paper. Two parameters, total suspended solids (TSS) and Secchi disk depth (SDD), were chosen for primary consideration. TSS (also known as seston) gives a measure of both organic (living and non-living) and inorganic suspended particulates, expressed in units of mass/volume ($mg\,l^{-1}$). SDD is the depth beyond which white (or white and black) disk suspended in the water body is no longer visible from the surface, expressed in units of length (m). SDD is a commonly used index of water transparency that incorporates both the absorption and backscattering characteristics of the water body.

2. Methods

2.1. *Study area*

The study area used in this investigation covers approximately the southern two-thirds of Green Bay and the adjacent waters of western Lake Michigan (figure 1). Green Bay contains a gradient of trophic states from hypereutrophic conditions at its southern end to oligotrophic conditions at the northern end; thus acting as a microcosm for the Great Lakes as a whole. The major influx of nutrients and sediments that maintains this gradient is the outflow of the Fox River, which enters at the Bay's southern end (figure 1). Owing to the polluted nature of the Fox River water, its transport and dispersal have a significant effect on the Bay's biota (Auer *et al.* 1986, Richman *et al.* 1984).

2.2. *Data aquisition*

The study period included four dates of observation between July 1984 and October 1987 (table 1). Concurrent surface reference and satellite sensor data sets were acquired on these four dates (figure 1). Depending on the available resources (personnel and equipment) the sample size (the number of sample stations) varied (table 1). The Landsat TM imagery were acquired at approximately 11.00 a.m. Central Daylight Time (CDT). The TM data were radiometrically and geometrically corrected. Sky conditions at the time of image acquisiton were reasonably haze-free but certain dates had scattered cumulus and cirrus cloud cover. The study area was restricted to the western half of the TM scene (sensor look-angle away from the sun) to reduce the effects of sun glint. The water samples were collected within one and one half hours of the satellite overpass, between 9.30 and 12.30 CDT. A LORAN-C

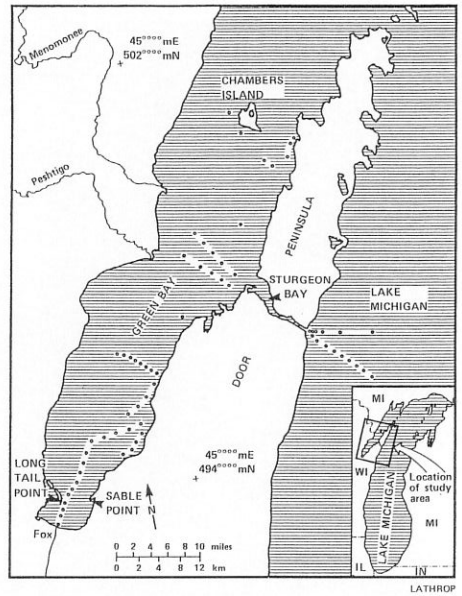

Figure 1. Map of study area with approximate locations stations. Note that not all stations were sampled on each acquisition data.

radionavigation system was used to establish the position (latitude and longitude) of each sample point to an accuracy of ± 460 m (U.S. Coast Guard 1984).

Water-quality reference data consisted of surface (to a depth of 0·3 m) measurements of total suspended solids ($mg\,l^{-1}$), Secchi disk depth (m), chlorophyll-a ($\mu g\,l^{-1}$), turbidity (NTU), absorbance (m^{-1}, at 0·375 μm) and temperature (°C) (see Appendix A). Data were collected in locations where potential bottom effects were avoided (the water depth was at least twice the Secchi disk depth).

2.3. *Satellite data extraction/evaluation*

The TM data for the three visible bands (Bands 1–3, centred on 0·485 μm, 0·570 μm, and 0·660 μm respectively) and one near-infrared band (Band 4, centred on 0·830 μm) were extracted at each sample point using the following procedure. First, a second-order polynomial coordinate transformation was used to relate ground

Table 1. Environmental conditions on dates of data acquisition.

Date	Wind direction	Wind speed ($km\,h^{-1}$)	Number of sample points
18 July 1984	NW	24	15
24 July 1986	SW	27	8
9 June 1987	NW	9	47
27 July 1987	S	12	15

positions in the Universal Transverse Mercator (UTM)] reference system to their equivalent row and column position in the TM scene. Second, the sample site locations in latitude and longitude were transformed to UTM and then to their corresponding satellite row/column addresses. Third, a high-resolution colour graphics monitor was then employed to locate and review each sample point in the imagery interactively. A 3×3 pixel window ($88{\cdot}5\,\text{m} \times 88{\cdot}5\,\text{m}$), centred on the sample point, was used to extract the digital numbers (DN) for each of the multispectral bands. These data were then averaged for each sample point on a band-by-band basis as a method of reducing sensor noise (Ritchie and Cooper 1987, Whitlock *et al.* 1982).

2.4. *Conversion of sensor digital number to reflectance*

The digital number (DN) data for each of the four TM bands (Appendix A) were first converted to spectral radiance, L_λ, ($\text{mW cm}^{-2}\,\text{sr}^{-1}\,\mu\text{m}^{-1}$). This conversion was done to transform the data from all the bands to the same physical units, as the DN scales for each band are calibrated differently (Robinove 1982). To facilitate the intercalibration of TM with other remote-sensor data sets (e.g. SPOT High Resolution Visible sensor), it is necessary to transform the spectral radiance values of the various sensors to a common scale that corrects for varying solar zenith angle, solar irradiance, sensor spectral band location and band width (Price 1987). Effective at-satellite reflectance, or in-band planetary albedo, a unitless measure, corrects for all these factors and was calculated using

$$R_\lambda = (\pi L_\lambda d^2)/(\text{ESUN}_\lambda \cos\theta_s) \tag{1}$$

where R_λ is the effective at-satellite reflectance (unitless); d is the Earth–Sun distance in astronomical units from nautical handbook; ESUN_λ is the mean solar exoatmospheric irradiance in $\text{mW cm}^{-2}\,\mu\text{m}^{-1}$ at wavelength λ; and θ_s is the solar zenith angle in degrees. The sensor calibration information needed for this process was taken from Markham and Barker (1986). The Earth–Sun distance, d, and solar zenith angle, θ_s are included in Appendix A.

2.5. *Reflectance data transformations*

A simple first-order atmospheric correction was implemented to evaluate between-date comparisons of reflectance values. A dark-pixel subtraction techique was used to correct for atmospheric path radiance. Clear oligotrophic lake or mid-ocean water is often used as a standard dark-pixel background and any radiance measured over such areas is assumed to be due solely to atmospheric path effects (Ahern *et al.* 1977, Gordon and Morel 1983). Path radiance is an additive term and once determined is subtracted from the total observed radiance before transforming the data to reflectance. Dark pixels located over the 'clear' central Lake Michigan waters were used as an estimate of path radiance for the entire scene. However, the assumption that the radiance measured from the 'clear' mid-lake waters in the shorter wavelength blue and green bands was due solely to path radiance may not be valid. The per-pixel technique of using the radiance measured in the red or near-infrared bands to correct for the corresponding blue and green bands was not possible in the more turbid waters of Green Bay because of the significant volume reflectance in the visible and near-infrared bands.

Ratioing of the multispectral image data can be used to suppress brightness variations within or between images, thus helping to extract spectral or colour information in the scene. However, ratios only compensate for those factors which operate equally across the bands and which are not additive in nature (i.e. the factors must cancel in the interband division). The utility of simple band ratios was examined using both dark-pixel corrected (dark-pixel subtraction before ratioing) and uncorrected reflectance data.

2.6. *Data analysis techniques*

Linear regression analysis was used to quantify the relations between the primary water-quality parameters (SDD and TSS) and selected bands and ratios of reflectance values. Several statistical parameters were used to indicate the significance of the regression models (Whitlock *et al.* 1982). These included the coefficient of determination (R^2), the standard error of the mean $\bar{Y}$ estimate (SE($\bar{Y}$)), and F value. The F value was expressed as a ratio of the observed F value to the critical F value at the 5 per cent significance level. A ratio greater than 4·0 implies a significant prediction equation (Draper and Smith 1981, Appendix 2C). Parsimonious regression models were stressed so as to aid in both their interpretation and their application by other potential users of the models.

The relations of nephelometric turbidity, chlorophyll-a, non-volatile suspended solids and absorbance with radiance/reflectance data were examined but not quantified through regression analysis. However, these other parameters were useful in assessing the relative importance of inorganic suspended solids, phytoplankton pigments and dissolved organic material in determining the water colour and volume reflectance.

The full data set was used to fit a multi-date calibration model. Thirty sample points were then randomly selected and excluded as a test set, the remaining sample points constituting a reduced data set were then used to develop a second calibration model. The randomly selected test data were then used to determine the root mean square error (RMSE) discrepancy between the predicted and observed values for the reduced data set (second) calibration model.

3. Results

An exponential model was found to typify the data best, resulting in the expression

$$y = a\exp(bx) \tag{2}$$

where y is the water-quality parameter of interest; x is the reflectance of selected band or ratio of reflectances in a band combination; and a and b are regression coefficients. A natural logarithmic transformation was required to linearize the data, such that

$$\ln y = \ln a + bx \tag{3}$$

This simple model accounted for most of the nonlinearity in the satellite sensor–surface reference data relationship. A nonlinear relation between suspended sediment concentration, turbidity and sensor reflectance has been reported by a number of other workers (Aranuvachapun and Walling 1988, Munday and Alfoldi 1979, Holyer 1978).

The surface reference data set is strongly intercorrelated (table 2). Green Bay represents a classic Case II situation with TSS, chlorophyll-a, and DOM (375 nm absorbance) levels positively covarying (Morel and Prieur 1977). Further examination of the correlation matrix shows high correlations of the individual band radiances and reflectances with the natural logarithms of transformed water-quality parameters (table 3). As expected, the correlation generally increased with increasing wavelength through the visible spectrum, peaked in the red band (TM band 3), and

then decreased in the near-infrared. The high TSS loads deposited in Green Bay by the Fox River are largely composed of inorganic suspended sediments (the non-volatile component of TSS), which strongly scatter and increase volume reflectance through the entire visible and near-infrared wavelengths (Bukata *et al.* 1985). The response in the visible and near-infrared bands is not as strong for the Lake Michigan portion of the data set where the TSS levels are an order of magnitude less (i.e. TSS $< 1{\cdot}0\,\mathrm{mg\,l^{-1}}$ or ln TSS $< 0{\cdot}0$) (figures 2(*a*)–(*d*)). Tassan (1987) found a similar cut-off in sensitivity in TM Band 3 data at suspended sediment levels of around $1\,\mathrm{g\,m^{-3}}$ (i.e. $1\,\mathrm{mg\,l^{-1}}$). As there is only a small range in solar zenith angle (from 54° to 58°), the conversion to reflectance does not improve the correlation of the satellite sensor–surface reference data set.

The ratioing of the reflectance data generally increased the degree of linear fit with surface reference data (table 3). The band 3/band 1 ratio (0·660 μm/0·485 μm) and to a lesser extent, the band 2/band 1 ratio (0·570 μm/0·485 μm) showed consistently high correlations for all the water-quality parameters. Based on the statistical parameters examined, the band 3/band 1 ratio (0·660 μm/0·485 μm) was selected as the 'best' band combination for the multi-date TSS and SDD calibration models (table 4). Overall, the significance of the multi-date models (i.e. R^2 values, F/F_{cr} ratios) are somewhat lower than those for single date models (when fit individually) but are still highly significant ($R^2 > 0{\cdot}86$) ($F/F_{cr} \gg 4{\cdot}0$) prediction equations (table 4). The accuracy of the estimate is generally within ±10 per cent for the mean Y. As with all regression models, the accuracy decreases at the extremes of the calibration data range. In this case, ±15 per cent at the lower ranges and due to the exponential nature of the models, ±25 per cent at the upper ranges.

When the reduced data set (training set) is analysed (minus the 30 points excluded as a test set), the regression coefficients (a and b) are not significantly different from the full model (table 4 (*b*)). The reduced data set model was then used to test the fit of the excluded test set. The estimated standard deviations for the fitted models for TSS and SDD (RMSE of the predicted *versus* observed values) respectively are TSS, $\pm 1{\cdot}3\,\mathrm{mg\,l^{-1}}$ for a range of 0·5–32·5 $\mathrm{mg\,l^{-1}}$ and SDD, ±1·2 m for a range of 0·5–9·0 m.

The dark-pixel-corrected reflectance data, including ratioed data, showed somewhat decreased correlations with the water quality parameters (table 3). Overall, the use of dark-pixel subtraction (on a per-scene basis) for a first-order atmospheric path radiance correction does not greatly improve the fit of the multi-date TM data set above that provided by ratio transforms.

Figures 2 and 3 show the efficacy of the band 3/band 1 ratio in normalizing for scene-to-scene differences. Examination of figures 2 (*a*) and 3 (*a*) shows that the 24 July 1986 data set is offset from the main locus of points. This date of acquisition

Table 2. Multi-date natural logarithmic surface reference data correlation matrix.

	ln SDD	ln TSS	ln CHL	ln TRB
ln TSS	−0·968			
ln CHL	−0·936	0·963		
ln TRB	−0·913	0·882	0·845	
ln ABS	−0·766	0·818	0·820	0·708

Table 3. TM multi-date reflectance and natural logorithmic surface reference data correlation matrix. TSS and ABS data set: 26 July 1986, 9 June 1987, 27 July 1987.

	ln SDD	ln TRB	ln CHL	ln TSS	ln ABS
Radiance					
Band 1	−0·549	0·568	0·473	0·532	0·392
Band 2	−0·730	0·736	0·617	0·679	0·470
Band 3	−0·844	0·796	0·777	0·824	0·637
Band 4	−0·653	0·591	0·625	0·719	0·587
Reflectance					
Band 1	−0·532	0·544	0·455	0·511	0·382
Band 2	−0·711	0·715	0·600	0·657	0·459
Band 3	−0·824	0·777	0·758	0·802	0·623
Band 4	−0·674	0·585	0·617	0·710	0·582
Band 3/band 1	−0·927	0·840	0·866	0·932	0·727
Band 2/band 1	−0·839	0·827	0·704	0·686	0·764
Band 3/band 2	−0·659	0·522	0·699	0·783	0·725
Dark-pixel-corrected reflectance					
Band 1	−0·362	0·438	0·164	0·219	−0·042
Band 2	−0·616	0·660	0·441	0·486	0·211
Band 3	−0·751	0·753	0·590	0·633	0·329
Band 4	−0·578	0·597	0·481	0·555	0·290
Band 3/band 1	−0·674	0·529	0·724	0·825	0·783
Band 2/band 1	−0·759	0·691	0·779	0·800	0·811
Band 3/band 2	−0·034	−0·141	0·022	0·149	0·176

was characterized by high haze levels and a higher background path radiance value. Ratioing of the reflectance data helped to correct for most of this difference (figures 2 (*b*) and 3 (*b*)).

Examination of figures 2 (*c*) and 3 (*c*) shows that the 27 July 1987 data set has a very different slope than the main locus of points. This same slope difference is evident in the uncorrected band 3 reflectance data as well (figures 2 (*a*) and 3 (*a*)), but

Table 4. Final regression results: multi-date TM data set. Regression model: $Y = a\exp(bx)$. (*a*) Full, (*b*) reduced data set.

Parameter	a	b	Bands	R^2	F/F_{cr}	n	95 per cent CI for the mean Y
(*a*) *Uncorrected reflectance data*							
SDD	192	−9·71	3/1	0·86	73	85	(2·5, 2·8)
TSS	0·0167	12·3	3/1	0·87	113	70	(3·2, 3·8)
Dark pixel corrected reflectance data							
SDD	11·8	−1·18	3/1	0·45	17	85	(2·3, 3·0)
TSS	0·340	1·96	3/1	0·68	36	70	(3·0, 3·9)
Parameter	a	b	Band	R^2	F/F_{cr}	n	r.m.s.e.
(*b*) *Uncorrected reflectance data*							
SDD	208	−9·82	3/1	0·87	86	55	1·2 m
TSS	0·0125	12·9	3/1	0·88	66	40	1·3 mg/l

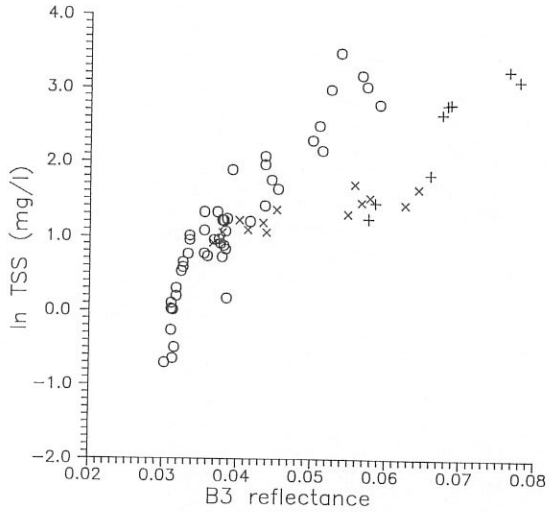

(*a*)

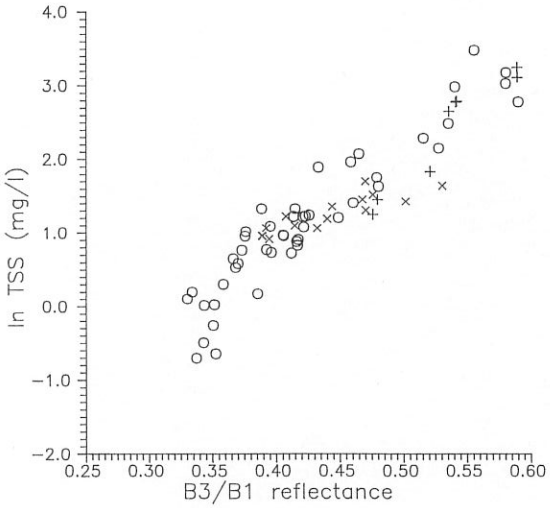

(*b*)

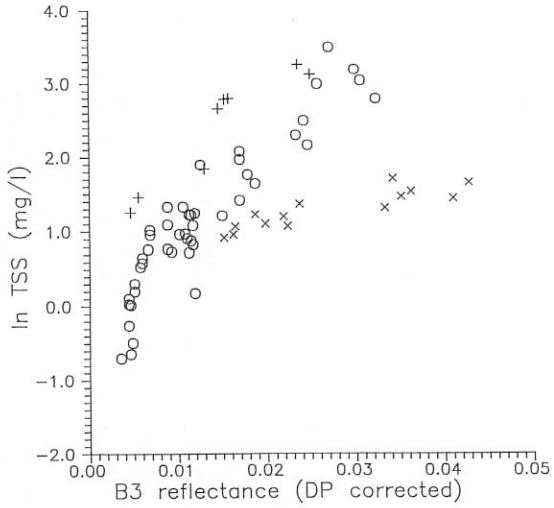

(*c*)

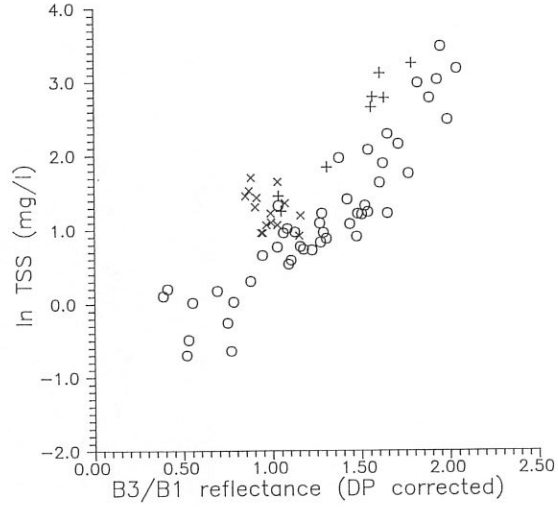

(*d*)

Figure 2. Plot of natural-logarithm-transformed total suspended solids (TSS) against TM reflectance for combined multi-date data set. Symbols: (*), 18 July 1984; (+), 24 July 1986; (○), 9 June 1987; and (×), 27 July 1987.

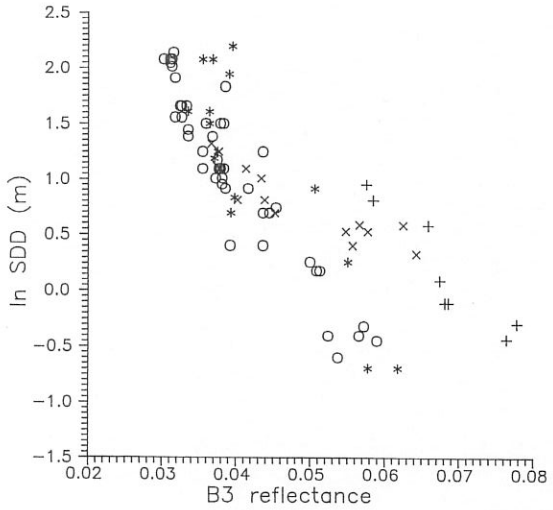

(*a*)

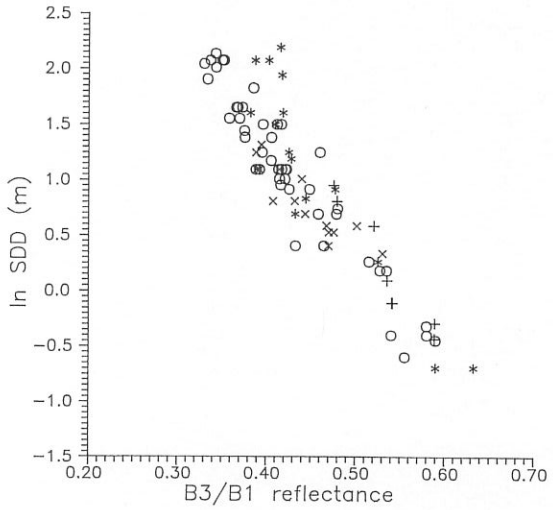

(*b*)

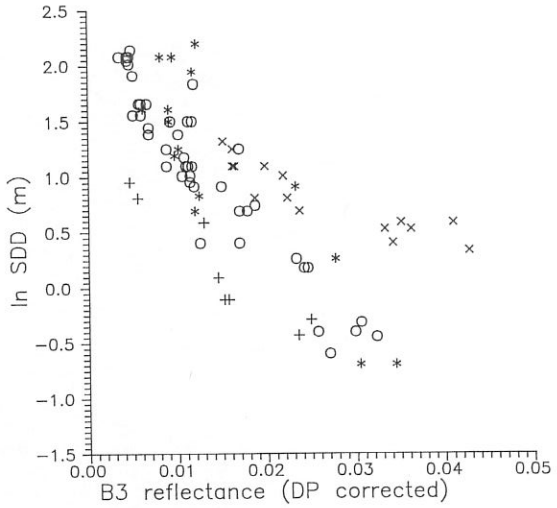

(*c*)

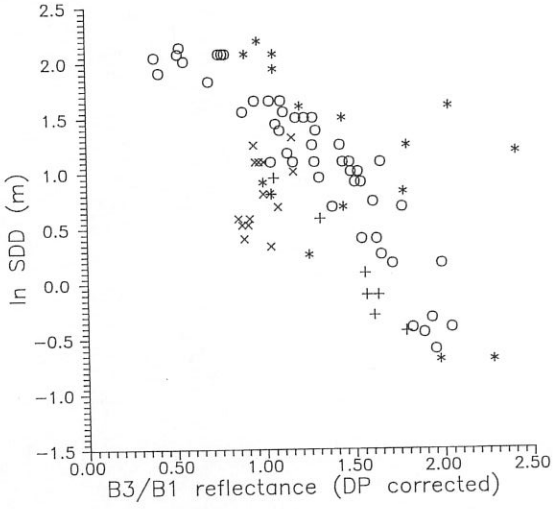

(*d*)

Figure 3. Plot of natural-logarithm-transformed Secchi disk depth (SDD) against TM reflectance for combined multi-date data set. (*a*) Plot of ln SDD against band 3 reflectance. (*b*) Plot of ln SDD against band 3/band 1 reflectance ratio. (*c*) Plot of ln SDD against band 3 reflectance (dark-pixel-corrected). (*d*) Plot of ln SDD against band 3/band 1 reflectance ratio (dark-pixel-corrected).

to a much lesser extent in the band 3/ band 1 ratio data (figures 2 (*b*) and 3 (*b*)). Ratioing of the dark-pixel-corrected reflectance data further isolates this data set as unique (figures 2 (*d*) and 3 (*d*)). This date of acquisition had turbid water conditions well up into the upper bay, apparently due to an extensive phytoplankton bloom (the only date that this situation occurred). Unfortunately, the lower half of the bay was obscured by heavy cloud cover, so a large range in surface reference data was not available (i.e. the Fox River plume with its elevated inorganic SS load). The unexplained behaviour of the 27 July 1987 data set points to the weakness of the empirical calibration approach in its inability to completely untangle the optical complexity of Green Bay's turbid waters.

4. Discussion

The turbid waters of Green Bay represent a classic Case II situation with covarying concentrations of inorganic suspended solids (SS), chlorophyll-a, and DOM. The high total suspended solids (TSS) loads ($>10\,mg\,l^{-1}$), including both inorganic and organic solids contributed by the Fox River (and possible wind re-suspension of lower bay sediments) appear to be the overwhelming determinant of the observed volume reflectance.

The concentration of non-volatile suspended solids, an indicator of SS, is well above the $0{\cdot}5\,mg\,l^{-1}$ level that Bukata *et al.* (1985) indicated would curtail the sensitivity of the water volume reflectance to changes in chlorophyll-a concentration. Further, the TM-measured reflectances show no evidence of chlorophyll absorption features similar to those observed under Case I oceanic conditions (Gordon and Morel 1983) (i.e. absorption of blue and red wavelengths with increasing chlorophyll-a, just the reverse is true). Under the highly turbid conditions experienced in Green Bay, the separate delineation of chlorophyll-a levels with the limited spectral resolution afforded by TM, should only be made with caution. The high levels of DOM input by the Fox River appear to affect volume reflectance in the lower portions of the bay where absorbance (at $0{\cdot}375\,\mu m$) levels are a factor of two higher than elsewhere in the bay or adjoining waters of Lake Michigan. High levels of DOM suppressed the volume reflectance in the visible bands, especially in the $0{\cdot}485\,\mu m$ wavelength band (TM band 1), but did not greatly affect the utility of the band 3/ band 1 ($0{\cdot}660\,\mu m/0{\cdot}485\,\mu m$) ratio.

5. Conclusions

A simple exponential model employing the band 3/band 1 ($0{\cdot}660\,\mu m/0{\cdot}485\,\mu m$) ratio was found to provide a useful multi-date TM water-quality calibration model for turbid inland water (Case II) conditions. As backscattering due to TSS increases, reflectance increases across all the visible and near-infrared wavelengths with the peak spectral response shifted to the long red wavelengths. The band 3/band 1 ratio takes advantage of this differential volume reflectance and provides a useful index of water transparency that is highly correlated with SDD and TSS levels.

TSS and SDD can be predicted with a reasonable degree of accuracy over most of their range (within approximately ± 10 per cent for the mean, as compared to an accuracy of ± 5 per cent due to sampling error alone). Owing to the exponential nature of the regression models, at higher parameter levels (i.e. near the upper limit of the calibration data) the prediction confidence interval widens considerably; the water-quality parameters can only be estimated to within ± 25 per cent.

Though these simple multi-date calibration algorithms have proven reasonably accurate in this study there are significant scene-to-scene differences that are uncompensated for by the band ratioing or dark-pixel subtraction. In the Great Lakes (and especially in Green Bay), the use of 'clear-water' radiance as dark pixels for simple path radiance correction is hampered by turbid water and the consequent high volume reflectances in the red and near-infrared wavelengths. A more sophisticated atmospheric correction algorithm may have provided better results (MacFarlane and Robinson 1984) but was beyond the scope of this study.

The calibration models developed in this study have been used to map SDD and TSS levels throughout the study area and coupled with calibrated thermal infrared imagery for surface water temperature (Lathrop and Lillesand 1987) have provided useful information in analysing Green Bay circulation patterns and the fate of the Fox River plume (Lathrop *et al.* 1990).

Acknowledgments

The water-quality data used in this study were collected with the assistance of John Vande Castle, James Buchholtz, John Eriksson, Karen Johnson, Philip Keillor, John Kennedy, Alison Kisch, He Ping, Paul Sager and Larry Siedl. John Vande Castle made many valuable contributions throughout this study. Paul Curran provided useful editorial advice. This research was funded primarily by the University of Wisconsin Sea Grant College Program Institute under grants from the National Sea Grant College Program, NOAA, U.S. Department of Commerce, and from the State of Wisconsin, Federal grant NA84AA-D-00065, project number 144-Y322. Funding, in part, has also been provided by a grant from the William and Flora Hewlett Foundation to the UW-Madison Institute for Environmental Studies.

Appendix A

TM/Surface Reference Data. Here SDD is the Secchi disk depth; CHL is the chlorophyll-a; TRB is the nephelometric turbidity; TSS is the total suspended solids; NVL is the nonvolatile SS; and ABS is the absorbance.

Appendix A1
18 July 1984 TM/surface reference data

Station	SDD (m)	CHL (μg/l)	TRB (NTU)	Digital number 1	2	3	4
1	0·5	48·6	10·0	83·8	31·4	30·3	14·9
2	0·5	49·6	10·7	83·6	32·4	32·0	14·0
3	2·3	7·9	1·6	76·8	24·7	21·2	10·9
4	3·3	7·2	1·1	74·3	23·3	19·8	11·1
5	3·5	5·3	0·95	75·7	23·7	20·0	12·0
6	2·0	13·6	1·6	77·9	26·0	20·9	11·3
7	4·5	4·3	0·85	76·2	23·4	19·4	11·1
8	5·0	4·4	0·75	75·2	22·6	18·0	10·0
9	5·0	4·1	1·0	74·7	22·9	19·4	11·0
10	1·3	4·9	7·9	89·4	33·1	28·7	15·2
11	2·5	3·4	3·3	90·4	32·2	26·4	14·1
12	7·0	1·5	0·95	80·2	25·0	20·8	12·0
13	9·0	1·5	0·75	81·4	25·7	21·0	12·8
14	8·0	1·1	0·69	78·4	24·0	19·7	12·2
15	8·0	2·7	0·57	78·6	24·1	19·0	12·0

Solar elevation angle: 56°.
Earth–Sun distance 1·0162898 astronomical units.

Appendix A2
24 July 1986 TM/surface reference data.

Station	SDD (m)	CHL ($\mu g l^{-1}$)	TRB (NTU)	TSS ($mg l^{-2}$)	NVL ($mg l^{-1}$)	ABS (m^{-1})	Digital number 1	2	3	4
	0·65	84·4	13·0	25·9	12·4	5·5	107·7	39·8	38·3	20·4
2	0·75	71·0	11·3	22·6	11·7	6·0	108·0	40·3	37·7	17·9
3	1·80	12·8	2·7	6·3	1·9	3·0	105·3	38·3	33·3	16·0
4	1·10	32·3	7·0	14·3	5·6	3·2	104·6	39·0	34·0	18·7
5	0·90	30·6	9·0	16·2	7·8	—	104·6	39·3	34·3	17·3
6	2·60	7·7	2·0	3·5	1·1	2·7	100·6	33·9	29·2	14·7
7	2·25	10·6	2·5	4·3	1·1	3·3	101·3	34·2	29·7	15·0
8	0·90	31·2	8·7	16·4	6·5	3·4	105·1	39·4	34·6	19·0

Solar elevation angle 54°.
Earth–Sun distance 1·0158322 astronomical units.

NB. Appendix A3 will be found on p. 2060.

Appendix A4
27 July 1987 TM/surface reference data.

Station	SDD (m)	CHL ($\mu g l^{-1}$)	TRB (NTU)	TSS ($mg l^{-1}$)	NVL ($mg l^{-1}$)	ABS (m^{-1})	Digital number 1	2	3	4
3	3·0	6·1	2·0	2·6	0·5	1·2	82·0	28·7	19·9	8·1
4	3·0	6·3	1·6	2·9	0·7	1·2	81·9	28·2	20·0	9·0
5	3·0	6·2	1·8	3·0	0·7	1·3	84·3	29·1	21·7	8·6
6	3·8	5·6	1·4	2·5	0·5	1·2	78·8	26·5	19·4	9·5
7	2·2	7·1	3·5	3·4	1·0	1·3	83·4	29·3	21·1	9·7
8	2·2	6·3	3·8	2·9	0·5	1·4	85·8	31·0	22·9	10·2
10	1·3	13·9	6·2	7·0	2·7	1·9	106·2	43·3	35·7	15·6
12	1·4	12·1	6·6	6·0	2·2	1·8	104·9	43·0	35·7	19·7
15	1·8	8·1	4·0	4·3	1·6	1·4	101·9	40·1	29·1	12·5
16	1·7	7·2	6·1	3·7	1·1	1·4	98·1	39·6	28·2	12·1
17	1·4	10·1	5·2	5·2	2·1	1·4	102·0	40·6	32·9	16·0
18	1·7	7·8	9·5	4·6	1·6	1·5	102·1	40·9	29·7	14·2
19	1·8	7·6	4·2	4·2	1·6	1·4	104·8	42·3	32·0	14·6
20	1·5	9·6	4·8	5·5	2·4	1·4	99·8	40·4	28·7	12·3
27	3·5	5·7	5·5	2·6	0·5	1·2	82·1	27·9	19·9	10·3
31	2·7	8·1	6·3	3·3	1·0	1·3	83·4	29·7	22·7	10·4
32	2·0	6·9	2·8	3·9	1·1	1·4	86·1	31·4	23·6	9·4
33	1·6	7·1	8·8	3·7	1·2	1·4	103·6	41·8	31·8	14·3
36	1·8	6·1	3·6	3·8	1·2	1·4	109·2	44·3	34·0	14·2
37	1·7	8·1	5·0	5·0	1·7	1·6	108·1	44·3	35·1	14·0
38	1·9	6·6	3·5	4·0	1·2	1·4	107·0	42·6	32·1	13·5
100	1·4	13·7	6·3	6·4	1·6	1·8	112·1	47·7	39·0	17·8

Solar elevation angle 55°.
Earth–Sun distance 1·0156631 astronomical units.

Appendix A3
9 June 1987 TM/surface reference data.

Station	SDD (m)	CHL ($\mu g l^{-1}$)	TRB (NTU)	TSS ($mg l^{-2}$)	NVL ($mg l^{-1}$)	ABS (m^{-1})	Digital number 1	2	3	4
0	4·0	8·6	1·5	2·6	0·3	2·0	79·7	25·7	20·1	11·0
1	3·2	5·0	1·8	2·6	0·6	2·0	81·1	25·2	20·4	11·2
2	4·5	4·1	1·8	2·1	0·4	1·8	80·8	25·8	20·7	10·6
3	4·5	4·4	1·4	2·1	0·4	1·9	79·7	25·8	19·7	11·3
4	4·5	5·0	1·8	2·3	0·4	2·0	80·8	26·7	20·9	11·8
5	3·5	9·2	2·4	4·1	1·6	2·1	83·1	28·9	23·6	13·0
6	1·5	15·9	3·4	8·0	4·1	2·5	82·3	28·4	23·6	13·0
7	1·3	16·8	4·2	9·9	4·5	2·6	85·0	31·0	26·8	13·8
8	2·0	13·2	2·8	7·1	3·8	2·3	83·4	29·2	23·6	13·1
9	2·1	10·7	2·3	5·1	2·1	2·2	82·9	29·7	24·4	13·1
10	2·0	10·6	3·2	5·8	2·8	2·4	81·6	28·8	24·0	12·8
11	3·0	7·1	2·8	3·8	1·4	1·9	80·2	25·9	19·4	11·0
12	3·5	5·2	1·8	3·0	0·9	1·9	78·9	25·1	19·4	10·4
13	2·8	8·8	2·6	3·8	1·5	2·1	78·9	26·1	20·3	10·6
14	2·5	8·6	2·2	3·5	0·4	2·1	79·6	25·8	21·0	10·7
15	3·0	8·4	2·2	3·4	1·0	2·2	80·4	26·3	20·7	11·2
16	3·0	6·3	1·9	2·9	0·8	3·3	79·9	26·1	20·9	11·3
17	2·8	7·5	2·4	3·4	1·0	2·0	79·6	25·9	20·8	11·4
18	3·0	5·2	3·0	3·4	1·5	1·9	78·8	26·6	20·7	12·0
19	1·5	8·0	4·3	6·7	3·9	2·0	79·6	26·6	21·3	11·8
20	3·0	3·8	1·7	2·2	0·4	2·1	79·4	25·9	19·4	12·0
21	4·2	6·3	1·6	2·6	0·9	1.8	78·4	24·7	18·4	11·0
22	4·0	6·4	1·4	2·8	1·0	1·7	78·3	24·1	18·4	10·6
23	4·8	4·6	1·2	1·8	0·5	1·6	77·6	24·1	18·0	8·1
24	5·2	3·5	1·5	1·9	0·6	1·7	78·3	24·3	18·0	8·6
25	5·2	3·6	1·8	2·2	0·6	1·7	78·4	24·3	18·3	9·1
26	5·2	5·8	1·2	1·7	0·1	1·8	77·4	24·1	17·9	10·9
27	7·5	2·4	2·8	1·0	0·3	0·4	80·1	23·1	17·3	8·8
28	8·5	2·2	0·90	0·6	0·0	0·4	80·8	24·0	17·4	9·2
29	7·8	1·5	0·55	1·1	0·3	0·5	82·7	24·8	17·2	11·6
30	6·8	1·4	0·70	1·2	0·3	0·3	83·4	25·1	17·6	10·9
31	8·0	1·8	0·45	1·0	0·0	0·2	77·8	23·1	17·2	8·7
32	8·0	1·6	0·55	0·8	0·0	0·3	78·0	23·4	17·2	8·4
35	6·2	2·0	0·90	1·2	0·3	0·3	87·6	27·5	21·0	14·8
36	4·8	4·4	1·30	1·4	0·0	1·7	77·9	23·8	17·6	10·7
39	8·0	1·9	0·40	0·5	0·0	0·3	78·8	23·3	16·8	10·2
40	8·0	2·2	0·65	0·5	0·0	0·6	78·1	22·1	17·3	8·4
100	3·0	7·2	3·8	2·5	0·0	1·9	79·3	25·9	20·6	10·3
101	2·6	6·6	7·2	2·4	0·0	1·9	80·4	25·7	20·8	10·7
102	2·5	9·3	2·6	3·4	0·3	2·0	81·4	28·9	22·6	11·0
103	1·2	17·9	5·0	8·6	3·4	2·8	85·2	32·1	27·4	12·6
104	1·2	14·6	6·3	12·1	5·8	3·0	83·3	31·9	27·2	11·7
105	0·64	36·8	14·0	16·2	8·9	3·3	87·6	34·3	31·3	13·1
106	0·73	35·8	10·5	20·8	11·0	3·2	86·4	34·1	30·4	13·1
107	0·67	58·9	4·5	24·1	12·2	5·2	85·4	33·1	30·1	14·9
108	0·55	85·6	16·5	32·6	16·9	4·9	84·8	31·6	28·7	13·9
109	0·67	66·4	9·9	19·8	7·5	5·7	85·0	31·4	28·0	13·8

Solar elevation angle 58°.
Earth–Sun distance 1·0150712 astronomical units.

References

AHERN, F. J., GOODENOUGH, D. G., JAIN, S. C., RAO, V. R., and ROCHON, G., 1977. Use of clear lakes as standard reflectors for atmospheric measurements. *Proceedings of the 11th International Symposium on Remote Sensing of Environment,* Ann Arbor, pp. 731–755.

ARANUVACHAPUN, S., and WALLING, D. E., 1988, Landsat-MSS radiance as a measure of suspended sediment in the lower Yellow River (Hwang Ho). *Remote Sensing of Environment,* **25,** 145–165.

AUER, M. T., KIESER, M. S., and CANALE, R. P., 1986, Identification of critical nutrient levels through field verification of models for phosphorus and phytoplankton growth. *Canadian Journal of Fishery and Aquatic Science,* **43,** 379–388.

BRICAUD, A., MOREL, A., and PRIEUR, L., 1981, Absorption by the dissolved organic matter of the sea (yellow substance) in the UV and visible domains. *Limnology and Oceanography,* **26,** 43–54.

BUKATA, R. P., JEROME, J. H., and BRUTON, J. E., 1988, Particulate concentrations in Lake St. Clair as recorded by a shipborne multispectral optical monitoring system. *Remote Sensing of Environment,* **25,** 201–229.

BUKATA, R. P., BRUTON, J. E., and JEROME, J. H., 1985, Application of direct measurements to the estimation of lake water quality indicators. *Environment Canada,* NWRI IWD Scientific Series No. 140 (Burlington, Ontario).

CARDER, K. L., STEWARD, R. G., HARVEY, G. R., and ORTNER, P. B., 1989, Marine humic and fulvic acids: their effects on remote sensing of ocean chlorophyll. *Limnology and Oceanography,* **34,** 68–81.

CURRAN, P. J., and NOVO, E. M. M., 1988, The relationship between suspended sediment concentration and remotely sensed spectral radiance: a review. *Journal of Coastal Research,* **4,** 351–368.

DRAPER, N. R., and SMITH, H., 1981, *Applied Regression Analysis* (New York: John Wiley).

GORDON, H. R., and MOREL, A. Y., 1983, *Remote Assessment of Ocean Color for Interpretation of Satellite Visible Imagery* (New York: Springer-Verlag).

HOLYER, R. J., 1978, Toward universal multispectral suspended sediment algorithms. *Remote Sensing of Environment,* **7,** 323–338.

JEFFREY, S. W., and HUMPHREY, G. F., 1975, New spectrophotometric equations for determining chlorophyll a, b, c1, and c2 in higher plants, algae and natural phytoplankton. *Biochemica Physiologia Pflanzen,* **167,** 191–194.

LATHROP, R. G., VANDE CASTLE, J. R., and LILLESAND, T. M., 1990, Monitoring river plume transport and mesoscale circulation in Green Bay, Lake Michigan through satellite remote sensing. *Journal of Great Lakes Research,* **16,** 471–484.

LATHROP, R. G., and LILLESAND, T. M., 1987, Calibration of Thematic Mapper thermal data for water surface temperature mapping: case study on the Great Lakes. *Remote Sensing of Environment,* **22,** 297–307.

LATHROP, R. G., VANDE CASTLE, J. R., and LILLESAND, T. M., 1990, Monitoring river plume transport and mesoscale circulation in Green Bay, Lake Michigan through satellite remote sensing, *Journal of Great Lake Research,* **16,** 471–484.

MACFARLANE, N., and ROBINSON, I. S., 1984, Atmospheric correction of Landsat MSS data for a multidate suspended sediment algorithm. *International Journal of Remote Sensing,* **5,** 561–576.

MARKHAM, B. L., and BARKER, J. L., 1986, Landsat MSS and TM post-calibration dynamic ranges, exoatmospheric reflectances and at-satellite temperatures. *EOSAT Landsat Technical Notes,* **1,** 3–8.

MOREL, A., and PRIEUR, L., 1977, Analysis of variations in ocean color. *Limnology and Oceanography,* **22,** 709–722.

MUNDAY, J. C., and ALFOLDI, T. T., 1979, Landsat test of diffuse reflectance models for aquatic suspended solids measurement. *Remote Sensing of Environment,* **8,** 169–183.

PRICE, J. C., 1987, Calibration of satellite radiometers and the comparison of vegetation indices. *Remote Sensing of Environment,* **21,** 15–27.

RICHMAN, S., SAGER, P. E., BANTA, G., HARVEY, T. R., and DESTASIO, B. T., 1984, Phytoplankton standing stock, size distribution, species composition and productivity along a trophic gradient in Green Bay, Lake Michigan. *Verhein International Verein Limnology,* **22,** 460–469.

RITCHIE, J. C., and COOPER, C. M., 1987, Comparison of Landsat MSS pixel array sizes for estimating water quality. *Photogrammetric Engineering and Remote Sensing,* **53,** 1549–1553.

ROBINOVE, C. J., 1982, Computation with physical values from Landsat digital data. *Photogrammetric Engineering and Remote Sensing,* **48,** 781–784.

TASSAN, S., 1987, Evaluation of the potential of the Thematic Mapper for marine application. *International Journal of Remote Sensing,* **8,** 1455–1478.

U.S. Coast Guard, 1984, LORAN-C accuracy. *Radionavigation Bulletin,* **15,** 3–9.

WHITLOCK, C. H., KUO, C. Y., and LECROY, S. R., 1982, Criteria for the use of regression analysis for remote sensing of sediment and pollutants. *Remote Sensing of Environment,* **12,** 151–168.